European Journal of Control xxx (xxxx) xxx

Contents lists available at ScienceDirect

European Journal of Control

journal homepage: www.sciencedirect.com/journal/european-journal-of-control

Data-driven LPV control based on Quadratic Matrix Inequalities: Experimental application to the Quanser Aero

Michelangelo Faleschini [a,b,*], Damiano Rotondo [c], Maria Letizia Corradini [a]

[a] School of Science and Technologies, Mathematics Division, University of Camerino, Via Madonna delle Carceri, Camerino (MC), 62032, Italy
[b] DIAG, Department of Computer, Control and Management Engineering, Sapienza University of Rome, Via Ariosto 25, Rome, 00185, Italy
[c] Department of Electrical and Computer Engineering (IDE), University of Stavanger, Stavanger, 4009, Norway

ARTICLE INFO

Recommended by T. Parisini

ABSTRACT

This paper presents the application of a recently proposed data-driven Linear Parameter Varying (LPV) controller design method to the Quanser Aero. The employed approach is based on Quadratic Matrix Inequalities (QMIs) and the strict matrix S-lemma. The existing approach is tweaked with the aim of forcing a higher control aggressiveness. Simulation and experimental results involving stabilization and multi-step-reference tracking are used to illustrate the validity and performance of the design.

1. Introduction

The Linear Parameter Varying (LPV) control theory is a modern control method that has been widely used in the design of control systems for complex and uncertain dynamic systems. During the recent years, great research efforts have been spent on LPV models, resulting in plenty of outcomes. For instance, efficient approaches have appeared that provided direct LPV models for gain-scheduling without requiring the laborious process of nonlinear system modeling or identification. Moreover, LPV control has gained greater attention during the 1990s, when the H_2 and H_∞ extensions based on Linear Matrix Inequalities (LMIs) from optimal control were published (see for example Scherer (1996)). Beside classical model-based LPV approaches, which require full system knowledge for controller and observer design (Apkarian, Gahinet, & Becker, 1995; Becker, Packard, Philbrick, & Balas, 1993; Devaprakash, Fry, & Farhood, 2019), several data-driven methods have emerged in recent years (Bachnas, Toth, Mesbah, & Ludlage, 2014), including behavioral LPV control for nonlinear systems (Verhoek, Abbas, & Tóth, 2023; Verhoek, Tóth, & Abbas, 2024) and a similar approach with parameter-dependent Lyapunov function to reduce conservatism (Verhoek, Eising, Dörfler, & Tóth, 2024).

In this paper, we focus on one of the latest data-driven LPV approaches (Miller & Sznaier, 2023), based on Quadratic Matrix Inequalities (QMIs) and the matrix S-Lemma, and we provide its first practical experimental application to the Quanser Aero system. The Quanser Aero system is a remarkable compact didactic-oriented dual-rotor machine designed for research and education purposes in control theory and robotics.

The contributions of our work are the following:

- the first experimental application of the data-driven LPV design algorithm proposed by Miller and Sznaier (2023), with an in-depth data-driven laboratory analysis of the Quanser Aero system;
- the modification of the approach described in Miller and Sznaier (2023) with the aim of forcing a higher control aggressiveness;
- an analysis of the Lyapunov function's behavior in the experimental case, providing insights into the observed deviation from its typical theoretical evolution.

The remaining of the paper is structured as follows. Section 2 reports the discrete-time data-driven LPV control algorithm presented in Miller and Sznaier (2023). Section 3 briefly describes the Quanser Aero device. Section 4 depicts the chosen internal model for the Quanser Aero system and the used input data collected from the plant, and discusses the results of some experiments involving stabilization and multi-step-reference tracking problems. Finally, Section 5 draws the main conclusions.

1.1. Notation

The n-dimensional real vector space is $\mathbb{R}^n$. The set of real $m \times n$ matrices is $\mathbb{R}^{m\times n}$. The transpose of a matrix $\mathbf{M}$ is $\mathbf{M}^T$. The set of symmetric n-dimensional matrices is $\mathbb{S}^n$ and its subsets of positive semidefinite and

* Corresponding author at: DIAG, Department of Computer, Control and Management Engineering, Sapienza University of Rome, Via Ariosto 25, Rome, 00185, Italy.
E-mail address: michelangelo.faleschini@uniroma1.it (M. Faleschini).

https://doi.org/10.1016/j.ejcon.2025.101299
Received 4 June 2025; Accepted 8 July 2025
Available online 28 July 2025
0947-3580/© 2025 The Authors. Published by Elsevier Ltd on behalf of European Control Association. This is an open access article under the CC BY license (http://creativecommons.org/licenses/by/4.0/).

positive definite matrices are $\mathbb{S}^n_+$ and $\mathbb{S}^n_{++}$, respectively. The vertical and horizontal concatenations of compatible-dimensional matrices $\mathbf{A}$ and $\mathbf{B}$ are denoted by $[\mathbf{A};\ \mathbf{B}]$ and $[\mathbf{A},\ \mathbf{B}]$, respectively. The matrices $\mathbf{I}_n$ and $\mathbf{0}_{m\times n}$ are the n-dimensional identity matrix and the $m\times n$ zero matrix, respectively. The dimension subscripts will be omitted when obtainable from the context. The symbol $\otimes$ denotes the Kronecker product (Liu & Trenkler, 2008), and the symbol $\otimes_{\text{col}}$ denotes the column-wise Khatri–Rao product (Khatri & Rao, 1968), defined for some matrices $\mathbf{A}\in\mathbb{R}^{m\times n}$ and $\mathbf{B}\in\mathbb{R}^{p\times n}$ as $\mathbf{A}\otimes_{\text{col}}\mathbf{B}=\begin{bmatrix}\mathbf{a}_1\otimes\mathbf{b}_1 & \mathbf{a}_2\otimes\mathbf{b}_2 & \dots & \mathbf{a}_n\otimes\mathbf{b}_n\end{bmatrix}$, where $\mathbf{a}_1,\mathbf{a}_2,\dots,\mathbf{a}_n$ and $\mathbf{b}_1,\mathbf{b}_2,\dots,\mathbf{b}_n$ are the columns of matrices $\mathbf{A}$ and $\mathbf{B}$, respectively. Whenever required by space limitation, the symbol $\star$ will be used in matrices to denote the terms induced by symmetry.

2. Data-driven LPV control algorithm

This section reports and comments the main theoretical results from Miller and Sznaier (2023) that will be the theoretical framework under which we perform the data-driven design for the Quanser Aero.

Let us consider a discrete-time LPV system with parameter-affine matrix $\mathbf{A}$, constant matrix $\mathbf{B}$ and polytopic structure (Briat, 2015), described as follows:

$$\mathbf{x}_{k+1}=\left(\sum_{\ell=1}^{L}\mathbf{A}_\ell\rho_{k\ell}\right)\mathbf{x}_k+\mathbf{B}\mathbf{u}_k, \tag{1}$$

for some matrices $\mathbf{A}_\ell\in\mathbb{R}^{n\times n}$, $\ell=1,\dots,L$, where $\mathbf{x}_k\in\mathbb{R}^n$, $\mathbf{u}_k\in\mathbb{R}^m$ and parameter $\boldsymbol{\rho}_k=[\rho_{k1},\dots,\rho_{kL}]^T\in\Omega\subset\mathbb{R}^L$ for any discrete time k. Suppose that Ω is compact and that it is the convex hull of an appropriate set of N_v vertices $\{\boldsymbol{\omega}_v\}_{v=1}^{N_v}\subset\mathbb{R}^L$. Assume also that $\boldsymbol{\rho}_k$ is measurable for all time k and that matrices $\mathbf{A}_1,\dots,\mathbf{A}_L,\mathbf{B}$ are unknown but consistent with data collected from the plant.

Following the gain-scheduling approach, the control of (1) is based on vertex controllers $\mathbf{K}_v\in\mathbb{R}^{m\times n}$ defined at each vertex $\boldsymbol{\omega}_v$, hence the state feedback control law corresponding to each vertex is given by $\mathbf{u}_k=\mathbf{K}_v\mathbf{x}_k$, where the controller matrix $\mathbf{K}_v$ must be computed using only input–output data from the plant. Then, the gain-scheduled controller $\mathbf{u}_k=\mathbf{K}(\boldsymbol{\rho}_k)\mathbf{x}_k$ for $\boldsymbol{\rho}_k\in\Omega$, is defined as a convex combination of the vertex controllers:

$$\mathbf{K}(\boldsymbol{\rho}_k)=\sum_{v=1}^{N_v}c_{kv}\mathbf{K}_v, \tag{2}$$

where, for any fixed k, the coefficient vector $\mathbf{c}_k\in\mathbb{R}^{N_v}$ is a vector of nonnegative constants so that:

$$\sum_{v=1}^{N_v}c_{kv}=1,\quad \sum_{v=1}^{N_v}c_{kv}\boldsymbol{\omega}_v=\boldsymbol{\rho}. \tag{3}$$

Closing the loop in (1) with the control law $\mathbf{u}_k=\mathbf{K}(\boldsymbol{\rho}_k)\mathbf{x}_k$ and using (3) leads to the equation $\mathbf{x}_{k+1}=\left[\sum_{v=1}^{N_v}c_{kv}\left(\mathbf{A}_v+\mathbf{B}\mathbf{K}_v\right)\right]\mathbf{x}_k$, with:

$$\mathbf{A}_v:=\sum_{\ell=1}^{L}\omega_{v\ell}\mathbf{A}_\ell. \tag{4}$$

The goal is to use the controller (2) to quadratically stabilize the system (1), as stated by the following definition.

Definition 1. The control law $\mathbf{u}_k=\mathbf{K}(\boldsymbol{\rho}_k)\mathbf{x}_k$ with $\mathbf{K}(\boldsymbol{\rho}_k)$ given by (2) *quadratically stabilizes* the discrete-time system (1) if there exists a matrix $\mathbf{P}\in\mathbb{S}^n_{++}$ such that the LMI:

$$\begin{bmatrix}\mathbf{P} & (\mathbf{A}_v+\mathbf{B}\mathbf{K}_v)\mathbf{P}\\ \mathbf{P}(\mathbf{A}_v+\mathbf{B}\mathbf{K}_v)^T & \mathbf{P}\end{bmatrix}\succ 0, \tag{5}$$

holds for all $v=1,\dots,N_v$.

Let us now present the definition of QMI, the Quadratic Boundedness Property and the Strict Matrix S-Lemma (van Waarde, Camlibel, Eising, & Trentelman, 2023).

Definition 2. Given matrices $\mathbf{M}\in\mathbb{S}^n$ and $\mathbf{Z}\in\mathbb{R}^{n\times k}$, a Quadratic Matrix Inequality (QMI) is either the inequality $\mathbf{Z}^T\mathbf{M}\mathbf{Z}\succeq 0$ or the strict inequality $\mathbf{Z}^T\mathbf{M}\mathbf{Z}\succ 0$.

Moreover, given a symmetric $(n+k)$-by-$(n+k)$ block matrix:

$$\boldsymbol{\Phi}=\begin{bmatrix}\boldsymbol{\Phi}_{11} & \boldsymbol{\Phi}_{12}\\ \boldsymbol{\Phi}_{12}^T & \boldsymbol{\Phi}_{22}\end{bmatrix}, \tag{6}$$

with $\boldsymbol{\Phi}_{11}\in\mathbb{S}^n$ and $-\boldsymbol{\Phi}_{22}\in\mathbb{S}^k_+$, a matrix $\mathbf{X}\in\mathbb{R}^{n\times k}$ is said to satisfy the *Quadratic Boundedness Property* with respect to $\boldsymbol{\Phi}$, i.e., $\mathbf{X}\in\text{QBP}(\boldsymbol{\Phi})$, if the QMI:

$$\begin{bmatrix}\mathbf{I}_n\\ \mathbf{X}^T\end{bmatrix}^T\begin{bmatrix}\boldsymbol{\Phi}_{11} & \boldsymbol{\Phi}_{12}\\ \boldsymbol{\Phi}_{12}^T & \boldsymbol{\Phi}_{22}\end{bmatrix}\begin{bmatrix}\mathbf{I}_n\\ \mathbf{X}^T\end{bmatrix}\succeq 0 \tag{7}$$

holds. Instead, $\mathbf{X}$ satisfies the *Strict Quadratic Boundedness Property* with respect to $\boldsymbol{\Phi}$, i.e., $\mathbf{X}\in\text{SQBP}(\boldsymbol{\Phi})$, if (7) is a strict QMI.

Lemma 1 (*Strict Matrix S-Lemma, van Waarde et al. (2023), Cor. 4.13*)**.** *Consider a matrix $\mathbf{X}\in\mathbb{R}^{n\times k}$ and some matrices $\mathbf{M},\mathbf{N}\in\mathbb{S}^{m+k}$ with the same structure and properties of (6). Assuming that $\ker\mathbf{N}_{22}\subseteq\ker\mathbf{N}_{12}$ and that the Schur complement $\mathbf{N}/\mathbf{N}_{22}\in\mathbb{S}^n_+$, then the following conditions are equivalent:*

- *if $\mathbf{X}\in\text{QBP}(\mathbf{N})$, then $\mathbf{X}\in\text{SQBP}(\mathbf{M})$;*
- *there exist real numbers $\alpha\geq 0,\beta>0$ such that:*

$$\mathbf{M}-\alpha\mathbf{N}-\begin{bmatrix}\beta\mathbf{I}_m & \mathbf{0}\\ \mathbf{0} & \mathbf{0}_{k\times k}\end{bmatrix}\succeq 0.$$

Let us consider now the data-driven controller design problem. Consider again system (1) in which we may add a noise discrepancy $\mathbf{w}_k$ for all k, bounded by a fixed $\varepsilon>0$. Let us suppose that we have recorded a set of N samples so that for $k=0,\dots,N-1$ we get:

$$\mathbf{x}_{k+1}=\left(\sum_{\ell=1}^{L}\rho_{k\ell}\mathbf{A}_\ell\right)\mathbf{x}_k+\mathbf{B}\mathbf{u}_k+\mathbf{w}_k. \tag{8}$$

A convenient way to store this collected data is introducing a tuple of matrices $D=(\mathbf{X}_-,\mathbf{U},\boldsymbol{\mathcal{P}},\mathbf{X}_+)$, where:

$$\begin{aligned}\mathbf{X}_-&=[\mathbf{x}_0\ \ \mathbf{x}_1\ \ \dots\ \ \mathbf{x}_{N-1}],\\ \mathbf{U}&=[\mathbf{u}_0\ \ \mathbf{u}_1\ \ \dots\ \ \mathbf{u}_{N-1}],\\ \boldsymbol{\mathcal{P}}&=[\boldsymbol{\rho}_0\ \ \boldsymbol{\rho}_1\ \ \dots\ \ \boldsymbol{\rho}_{N-1}],\\ \mathbf{X}_+&=[\mathbf{x}_1\ \ \mathbf{x}_2\ \ \dots\ \ \mathbf{x}_N].\end{aligned}$$

Moreover, denoting by $\boldsymbol{\mathcal{P}}_\ell\in\mathbb{R}^{1\times N}$ the ℓ-th row of matrix $\boldsymbol{\mathcal{P}}$, it is possible to define the discrepancy matrix $\mathbf{W}$ associated to data D as follows:

$$\mathbf{W}=\mathbf{X}_+-\left(\sum_{\ell=1}^{L}\boldsymbol{\mathcal{P}}_\ell\otimes_{\text{col}}\mathbf{A}_\ell\right)\mathbf{X}_--\mathbf{B}\mathbf{U}.$$

The following will be assumed in what follows:

1. The positive integers n,m,L,N are finite and known.
2. The set Ω is a known compact non-empty polytope with vertices $\{\boldsymbol{\omega}_v\}_{v=1}^{N_v}$.
3. There exists a known matrix $\hat{\boldsymbol{\Phi}}\in\mathbb{S}^{n+N}$, with the structure and properties of (6), such that $\mathbf{W}\in\text{QBP}(\hat{\boldsymbol{\Phi}})$.

Remark 1. These assumptions are reasonable in practice. In fact, the first two assumptions follow naturally from the construction of the system internal model, as demonstrated in 4.1. The third assumption refers to a specific formulation of boundedness, which becomes useful for incorporating QMIs on the matrix $\mathbf{W}$. This assumption is also reasonable, as matrix $\mathbf{W}$ represents the gap between the real system next state value and the predicted next state value computed using the internal matrices $\mathbf{A}_\ell$ and $\mathbf{B}$, and the current state and input. Therefore, by choosing an internal LPV model of sufficiently high order, and leveraging the LPV systems ability to approximate complex nonlinear

systems, it is always possible to ensure boundedness of matrix $\mathbf{W}$. Specifically, the matrix $\hat{\boldsymbol{\Phi}} \in \mathbb{S}^{n+N}$ can be selected a priori to depend on the noise bound ϵ while still satisfying properties of (6), for instance as follows:

$$\hat{\boldsymbol{\Phi}} = \begin{bmatrix} \epsilon^2 N \mathbf{I}_n & \star \\ \mathbf{0}_{N\times n} & -\mathbf{I}_N \end{bmatrix}. \tag{9}$$

The aim is to constrain the matrix $\mathbf{W}$ as much as possible, and a convenient and simple to implement condition is formally expressed by the QBP.

From a particular reformulation of $\mathbf{W}$ (see Miller and Sznaier (2023) for details), let us define the matrix $\boldsymbol{\Psi} \in \mathbb{S}^{n+(Ln+m)}$ as follows:

$$\boldsymbol{\Psi} = \begin{bmatrix} \mathbf{I}_n & \mathbf{X}_+ \\ \mathbf{0}_{Ln\times n} & -\boldsymbol{\mathcal{P}} \otimes_{\text{col}} \mathbf{X}_- \\ \mathbf{0}_{m\times n} & -\mathbf{U} \end{bmatrix} \hat{\boldsymbol{\Phi}} \begin{bmatrix} \mathbf{I}_n & \mathbf{X}_+ \\ \mathbf{0}_{Ln\times n} & -\boldsymbol{\mathcal{P}} \otimes_{\text{col}} \mathbf{X}_- \\ \mathbf{0}_{m\times n} & -\mathbf{U} \end{bmatrix}^T. \tag{10}$$

The solution to the subproblem of finding the vertex controller $\mathbf{K}_v \in \mathbb{R}^{m\times n}$ that stabilizes the subsystem represented by $\mathbf{A}_v$ at vertex v is now given by the following result.

Theorem 1. *For any fixed $v = 1, \dots, N_v$, the LMI (5) holds if and only if there exist constants $\alpha_v \geq 0$ and $\beta_v > 0$ such that the matrix inequality:*

$$\begin{bmatrix} \mathbf{P} - \beta_v \mathbf{I}_n & \star & \star & \star \\ \mathbf{0}_{Ln\times n} & -(\boldsymbol{\omega}_v \boldsymbol{\omega}_v^T) \otimes \mathbf{P} & \star & \star \\ \mathbf{0}_{m\times n} & -\boldsymbol{\omega}_v^T \otimes \mathbf{S}_v & \mathbf{0}_{m\times m} & \star \\ \mathbf{0}_{n\times n} & \mathbf{0}_{n\times Ln} & \mathbf{S}_v^T & \mathbf{P} \end{bmatrix} - \alpha_v \begin{bmatrix} \boldsymbol{\Psi} & \star \\ \mathbf{0} & \mathbf{0}_{n\times n} \end{bmatrix} \geq 0. \tag{11}$$

holds, where $\mathbf{S}_v = \mathbf{K}_v \mathbf{P}$ and the matrix $\boldsymbol{\Psi}$ is given by (10).

Proof. It stems from Lemma 1 (see Miller and Sznaier (2023) for details). □

Finally, the discrete-time semidefinite program for the quadratic stabilization of (8) through gain-scheduled vertex controllers $\{\mathbf{K}_v = \mathbf{S}_v \mathbf{P}^{-1}\}_{v=1}^{N_v}$ is expressed as follows:

$$\begin{aligned} &\text{find } \mathbf{P} \in \mathbb{S}^n_{++}, \\ &\quad \boldsymbol{\alpha} \in \mathbb{R}^{N_v}_{\geq 0}, \boldsymbol{\beta} \in \mathbb{R}^{N_v}_{>0}, \\ &\quad \mathbf{S}_v \in \mathbb{R}^{m\times n} \quad \forall v = 1, \dots, N_v, \text{ such that} \\ &\quad \text{LMI(11)holds} \quad \forall v = 1, \dots, N_v. \end{aligned} \tag{12}$$

Solving (12) allows to obtain the matrices $\mathbf{P}$ and $\mathbf{S}_v$ for all $v = 1, \dots, N_v$, and consequently the gain-scheduled controller $\mathbf{K}(\boldsymbol{\rho}_k)$ for any k from the vertex controllers $\mathbf{K}_v$ through (2). To solve the latter program, YALMIP interface (see Lofberg (2004)) and Mosek solver (see ApS (2019)) will be used.

3. Quanser Aero

The Quanser Aero (Inc, 2016a) is a versatile dual-rotor machine developed by the Canadian company "Quanser Consulting Inc" and designed for research and education purposes in control theory and robotics (see Fig. 1). It is equipped with sensors, an embedded computer, and communication systems for real-time control and data collection. Based on the rotors angles, it offers three possible configurations:

- 1 degree of freedom (DOF) setup with horizontal-oriented rotors, also called *Half Quad* configuration;
- 1 DOF setup with vertical-oriented rotors;
- 2 DOF helicopter to half-quadrotor, in which one rotor is horizontal and the other one is vertical.

The Aero has three main parts: the base, which is a fixed box that provides a stable support for the whole structure; the support-yoke, which is the vertical and fork-like designed support; the upper body, which is composed by two metal pipes, with rotor blades at the end of each, connected to the support-yoke in such a way that the body can rotate between +54° and −62° with respect to the support-yoke. The angle described by the rotation of the support-yoke onto the base is called *yaw angle*, while the angle between the upper body and the horizontal axis is called *pitch angle*. The propellers are powered by DC motors, equipped with high-resolution optical encoders for velocity measurements, and the base has encoders on all rotational joints for measuring the pitch and yaw angles. Further information about the Aero system can be found in Inc (2016b).

In the following, the Quanser Aero in Half Quad configuration will be considered. Therefore, the system under consideration is a SISO system with a two-dimensional state vector. Particularly, the input is the voltage supplied to the DC motors installed in the two rotors and it is saturated to vary between −24 and +24 V; the output is the pitch angle assumed by the main body of the Aero with respect to the horizontal and it is captured by measurement sensors; the two state variables are the pitch angle and the pitch velocity, respectively. Moreover, it must be said that the Quanser Aero system is naturally stable, i.e. by dropping the Aero from any pitch angle, after a phase of free oscillation, it will autonomously return to the horizontal position with zero pitch angle. Similarly, starting from the horizontal position and applying a constant input voltage to the propellers, the Aero will autonomously stabilize at a certain pitch angle which depends on the supplied input voltage. Therefore, in order to appreciate the effect of a closed-loop controller applied to the system, the open-loop behavior of the system will be reported together with the corresponding closed-loop behavior.

4. Experiments

In this section, we report and discuss some experiments on the Quanser Aero in Half Quad 1 DOF configuration about the discrete-time data-driven LPV control algorithm.

4.1. Internal model for the Quanser Aero

To use the previously described discrete-time data-driven LPV algorithm, a model with structure as in (1) must be chosen a priori. The chosen approach is to assume a combination of two LTI models for low and high pitch angles and input voltages, respectively. With this aim in mind, let us choose $L = 2$ and suppose that the polytope $\Omega \subset \mathbb{R}^2$ is represented by a segment corresponding to the convex hull of the two vertices $\boldsymbol{\omega}_1 = [1, 0]^T, \boldsymbol{\omega}_2 = [0, 1]^T \in \mathbb{R}^2$. Then, the model is expressed as follows:

$$\mathbf{x}_{k+1} = \left(\rho_{k1}\mathbf{A}_1 + \rho_{k2}\mathbf{A}_2\right)\mathbf{x}_k + \mathbf{B}\mathbf{u}_k, \tag{13}$$

where matrices $\mathbf{A}_1$, $\mathbf{A}_2$ and $\mathbf{B}$ are implicitly computed internally to the data-driven process, and denoting by $\bar{\rho}$ and $\underline{\rho}$ respectively the upper and lower bounds of the pitch angle, the coefficients ρ_{k1} and ρ_{k2} are chosen as follows:

$$\rho_{k1} = \frac{\bar{\rho} - x_{k1}}{\bar{\rho} - \underline{\rho}} \qquad \text{and} \qquad \rho_{k2} = \frac{x_{k1} - \underline{\rho}}{\bar{\rho} - \underline{\rho}}, \tag{14}$$

where x_{k1} denotes the pitch angle of the Aero at time k. Notice that with the previous choice $\rho_{k1}, \rho_{k2} \geq 0$ and $\rho_{k1} + \rho_{k2} = 1$, hence $\boldsymbol{\rho}_k = [\rho_{k1}, \rho_{k2}]^T$ belongs to the polytope Ω defined above, which means that the state matrix of the model (13) is given by a convex combination of LTI state matrices. Moreover, for the gain-scheduled controller $\mathbf{K}(\boldsymbol{\rho}_k)$ in (2), let us choose $c_{k1} = \rho_{k1}$ and $c_{k2} = \rho_{k2}$.

4.2. Data collection

The subsequently-used data shown in Fig. 2 consist of a 60 s (i.e. $N = 1500$ samples with $T = 0.04$ second sampling time) collection involving a piecewise constant input that randomly changes between −24 and +24 volt every 0.2 s. In particular, each input u_k is randomly drawn from a uniform distribution over the interval $[-24, 24]$. Taking into account (14) and observing the first graph about the pitch angle, the upper bound $\bar{\rho} = 0.6$ and the lower bound $\underline{\rho} = -0.7$ have been assigned to define the range of variability of the pitch angle.

Fig. 1. Quanser Aero in the 2 DOF configuration (Inc, 2016b).

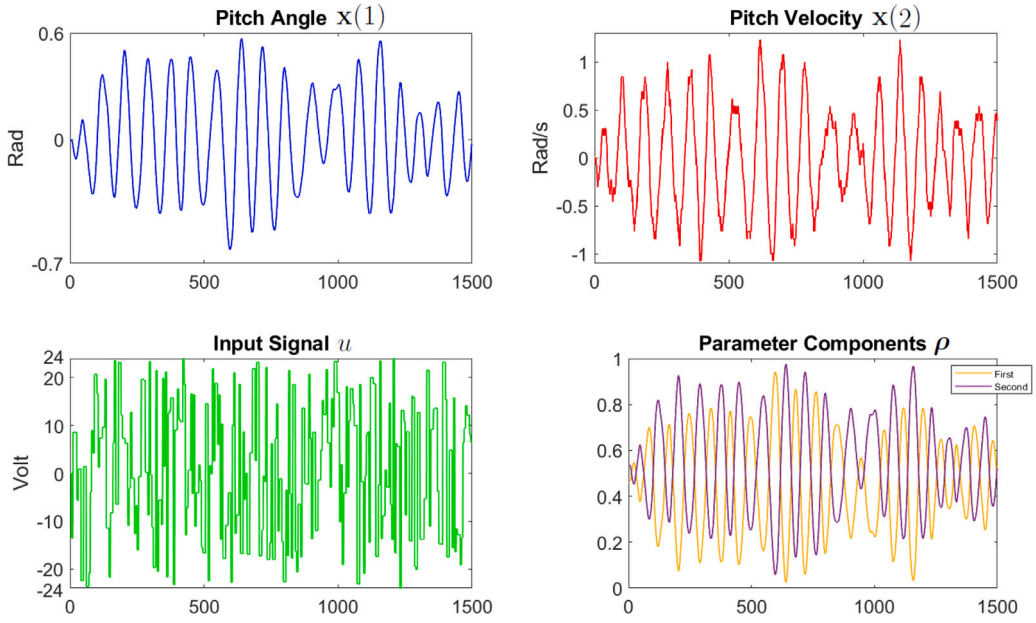

Fig. 2. Data collected from the Aero plant using a piecewise constant input that randomly changes between −24 and +24 volt every 0.2 s, for a total of 60 s of collection.

4.3. Results

4.3.1. Stabilization problem

Let us consider a stabilization problem, assuming that $\mathbf{x}_0 = [0.3, 0]^T$ and $\mathbf{x}_{ref} = [0, 0]^T$. Before presenting the results, it must be pointed out that the data-driven gain-scheduled controller designed using the approach proposed by Miller and Sznaier (2023) did not produce a substantial modification of the transient response of the Aero system, when compared to the open-loop response. With the goal of obtaining a controller gain which speeds up the transient and reduces the settling time, a more aggressive Lyapunov-based condition has been considered. More specifically, the condition $V(\mathbf{x}_{k+1}) - V(\mathbf{x}_k) < 0$ originally considered by Miller and Sznaier (2023) for the quadratic Lyapunov function $V(\mathbf{x}_k) = \mathbf{x}_k^T \mathbf{P}^{-1} \mathbf{x}_k$ (which led to (5) in Definition 1) has been replaced by the stronger requirement $V(\mathbf{x}_{k+1}) - V(\mathbf{x}_k) < -cV(\mathbf{x}_k)$ for a positive scalar $c \in [0, 1)$, thus demanding a higher rate of decay of the function V. Then, repeating the same procedure of Section 2 leads to the final program (12), where the first term in (11) is replaced by the following matrix[1]:

$$\begin{bmatrix} \mathbf{P} - \beta_v \mathbf{I}_n & \mathbf{0} & \mathbf{0} & \mathbf{0} \\ \mathbf{0} & -\frac{(\boldsymbol{\omega}_v \boldsymbol{\omega}_v^T) \otimes \mathbf{P}}{1-c} & -\frac{\boldsymbol{\omega}_v \otimes \mathbf{S}_v^T}{1-c} & \mathbf{0} \\ \mathbf{0} & -\frac{\boldsymbol{\omega}_v^T \otimes \mathbf{S}_v}{1-c} & \mathbf{0} & \mathbf{S}_v \\ \mathbf{0} & \mathbf{0} & \mathbf{S}_v^T & (1-c)\mathbf{P} \end{bmatrix}$$

Executing the algorithm for $c = 0$, $c = 0.1$, $c = 0.2$ and $c = 0.3$ produces the following vertex controllers, where the corresponding value of c is indicated in the superscripts:

$$\begin{aligned} \mathbf{K}_1^{(0)} &= \begin{bmatrix} -32.6 & -8.4 \end{bmatrix}, \mathbf{K}_2^{(0)} = \begin{bmatrix} -26.9 & -20.1 \end{bmatrix}; \\ \mathbf{K}_1^{(0.1)} &= \begin{bmatrix} -91.4 & -13.3 \end{bmatrix}, \mathbf{K}_2^{(0.1)} = \begin{bmatrix} -85.5 & -25.8 \end{bmatrix}; \\ \mathbf{K}_1^{(0.2)} &= \begin{bmatrix} -163.1 & -17.5 \end{bmatrix}, \mathbf{K}_2^{(0.2)} = \begin{bmatrix} -163.9 & -30.9 \end{bmatrix}; \\ \mathbf{K}_1^{(0.3)} &= \begin{bmatrix} -294.1 & -23.5 \end{bmatrix}, \mathbf{K}_2^{(0.3)} = \begin{bmatrix} -303.2 & -37.1 \end{bmatrix}. \end{aligned}$$

[1] Notice that when $c = 0$, the matrix appearing in (11) is recovered.

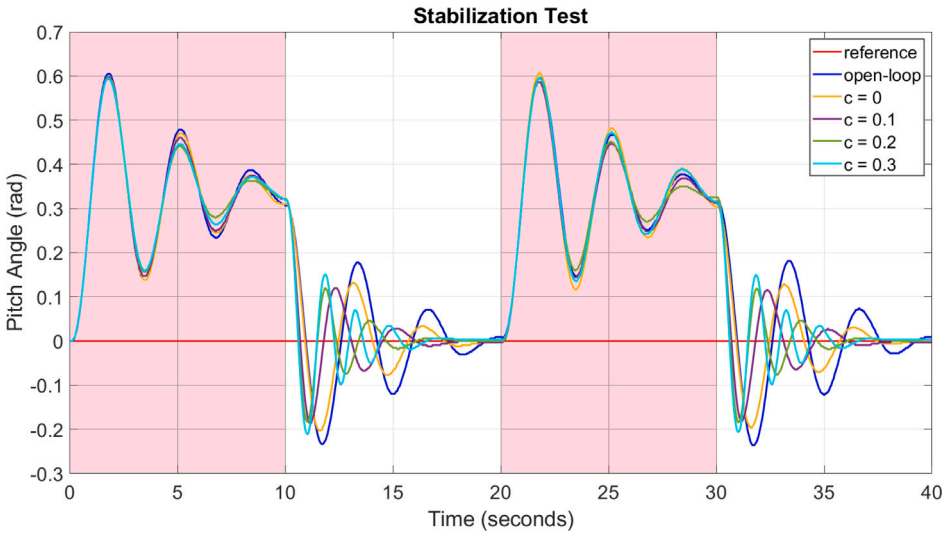

Fig. 3. Pitch angle response of the Quanser Aero: in the first 10 s and between 20 and 30 s (pink areas), the Aero is excited with a constant input of 20 volt; in the other intervals, the previous input is turned off and the stabilizing controllers are activated.

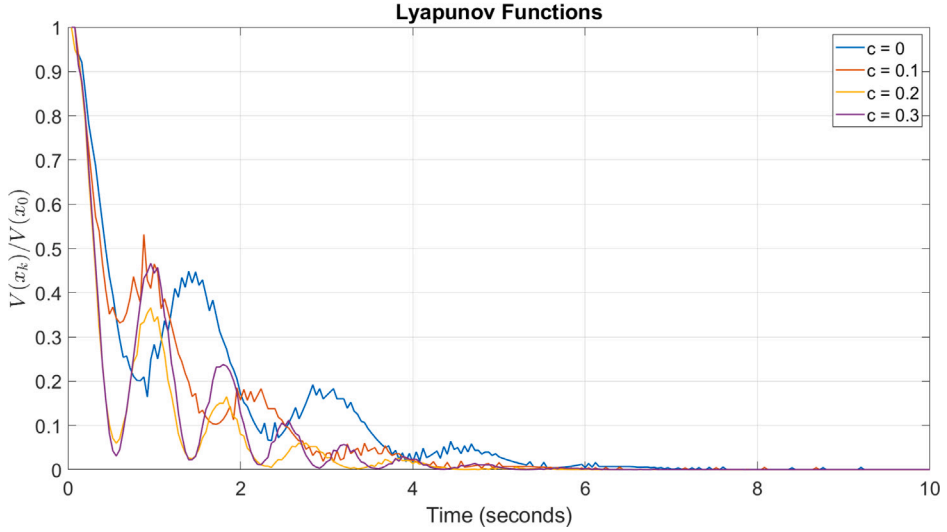

Fig. 4. Lyapunov functions trajectories corresponding to the previous stabilization problems with parameters $c = 0$, $c = 0.1$, $c = 0.2$ and $c = 0.3$, respectively.

Running the Aero with the four gain-scheduled controllers obtained by convex combination of the above vertex controllers leads to the results shown in Fig. 3. The corresponding measured 5% settling times are 9.8 (open-loop), 8.2, 7.1, 6.3 and 6.5 s, respectively. The control input ℓ^2-norms in the interval [10,20] seconds are 52.9, 109.0, 151.5 and 205.1, respectively, confirming the controller's increasing aggressiveness as c grows.

4.3.2. Lyapunov analysis

In the previous stabilization problem an overly aggressive controller does not seem to be very effective because it makes the pitch angle oscillate with a greater amplitude and higher speed, which is often not appropriate for real applications. These observed effects are due to the particular shape of the Lyapunov matrices $\mathbf{P}$ generated by the stabilizing algorithm, because of which, to make V decrease faster, the trajectories of the system prioritize the decrease of the pitch angle over the pitch velocity, which is instead free to be higher.

Let us also analyze the corresponding Lyapunov function behavior for the previous experiments in Fig. 4, focusing on the time interval $[10, 20]$ seconds and rescaling each function by its first value $V(\mathbf{x}_0)$ in order to provide a better comparison between each other. These Lyapunov functions decrease faster when c is higher, as expected, except for the case $c = 0.3$, where the rate of decrease of V appears to be lower compared to $c = 0.2$. Coherently, the measured settling time when $c = 0.3$ is higher compared to the case of $c = 0.2$.

Moreover, the Lyapunov functions in Fig. 4 behave unusually, oscillating during the decay phase, unlike in simulations. Indeed, theoretically the Lyapunov stability condition on the rate of decrease of V imposes that the function V must always decrease over time, but in those cases the Lyapunov functions oscillate increasing their value in some time interval, although they still maintain a decreasing behavior overall. Let us consider the first Lyapunov function for the case $c = 0$, for instance, and let us plot the system response trajectory and the Lyapunov level curves, i.e. the set of points $\mathbf{x}$ such that $V(\mathbf{x}) = \mathbf{x}^T\mathbf{P}^{-1}\mathbf{x} = r$ for different values of $r \in \mathbb{R}_+$, in the phase plane, as shown in Fig. 5. The picture illustrates the reason why the function V increases at some time interval, corresponding to the time when the phase plane system trajectory slightly deviates from some Lyapunov level curves.

A possible explanation of this behavior stems from the mismatch between the real Aero system dynamics and the internal LPV Aero model, since the simplified model (13) is not able to capture the nonlinearities that affect the real Aero's dynamics sufficiently well. To

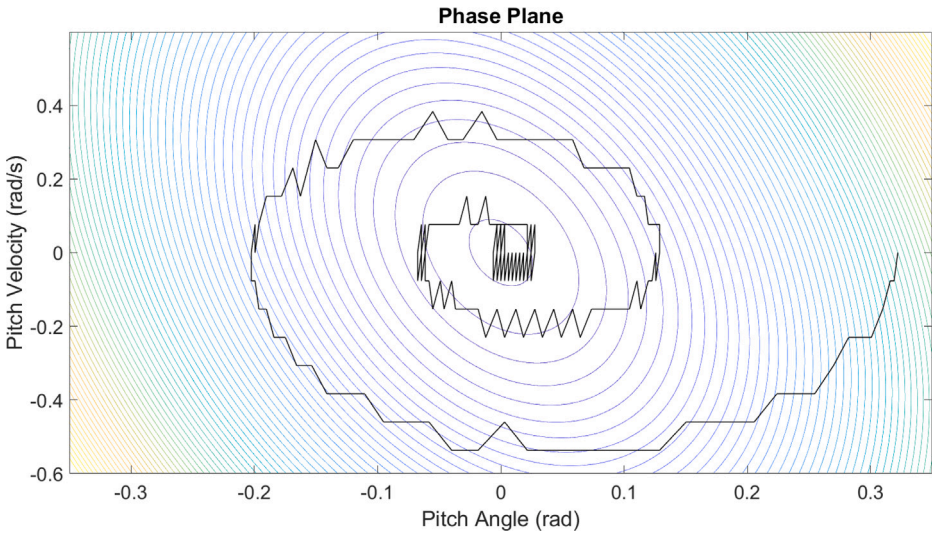

Fig. 5. Phase plane representing the Lyapunov level curves and the system response trajectory (in black) of the stabilization experiment with $c = 0$.

assess the plausibility of this statement, let us consider an LTI model obtained from input–output data, denoted as $\mathbf{A}_{\text{data}}$, and let us assume that the real system is described by a less-damped LTI model, $\mathbf{A}_{\text{real}}$. Since the system is already stable, it is possible to work with the open-loop system for simplicity, but analogous considerations could be done for the closed-loop system. The stability of $\mathbf{A}_{\text{data}}$ can be analyzed using a Lyapunov function $V(\mathbf{x}_k) = \mathbf{x}_k^T \mathbf{P} \mathbf{x}_k$ with $\mathbf{P} \in \mathbb{S}^n_{++}$. The condition for stability is given by:

$$\mathbf{A}_{\text{data}}^T \mathbf{P} \mathbf{A}_{\text{data}} - \mathbf{P} \prec 0,$$

which ensures that $V(\mathbf{x}_{k+1}) - V(\mathbf{x}_k) < 0$. Le us investigate whether the same matrix $\mathbf{P}$ guarantees the stability of the real system, $\mathbf{A}_{\text{real}}$.

Let us model $\mathbf{A}_{\text{real}}$ as a perturbed version of $\mathbf{A}_{\text{data}}$, introducing an error matrix $\Delta\mathbf{A}$ such that $\mathbf{A}_{\text{real}} = \mathbf{A}_{\text{data}} + \Delta\mathbf{A}$.

Substituting this into the Lyapunov stability condition and expanding the expression yields:

$$\mathbf{A}_{\text{data}}^T \mathbf{P} \mathbf{A}_{\text{data}} + \mathbf{A}_{\text{data}}^T \mathbf{P} \Delta\mathbf{A} + \Delta\mathbf{A}^T \mathbf{P} \mathbf{A}_{\text{data}} + \Delta\mathbf{A}^T \mathbf{P} \Delta\mathbf{A} - \mathbf{P} \prec 0$$

The first term is already negative since $\mathbf{P}$ stabilizes $\mathbf{A}_{\text{data}}$. However, the mixed terms $\mathbf{A}_{\text{data}}^T \mathbf{P} \Delta\mathbf{A}$ and $\Delta\mathbf{A}^T \mathbf{P} \mathbf{A}_{\text{data}}$, along with the quadratic term $\Delta\mathbf{A}^T \mathbf{P} \Delta\mathbf{A}$, represent the influence of the perturbation $\Delta\mathbf{A}$. If $\Delta\mathbf{A}$ is large, or if it introduces significant changes, these terms may render the Lyapunov function no longer always decreasing.

As practical evidence to support this claim, let us confirm it through a simulation. Using YALMIP interface and Mosek solver, let us compute a feasible Lyapunov matrix $\mathbf{P} \in \mathbb{S}^2_{++}$ such that Lyapunov stability condition above holds. Then, simulating two trajectories using the identified LTI model and the less-damped model (supposed to be the real one), the corresponding Lyapunov function are computed using the same matrix $\mathbf{P}$, as shown in Fig. 6. Notice that the Lyapunov function for the less-damped system has a behavior similar to that of the experimentally computed Lyapunov functions in Fig. 4.

4.3.3. Multi-step reference tracking problem

Finally, let us consider a multi-step-reference described by the sequence $[0.4, -0.1, 0.1, 0.2, -0.3, -0.2, 0.2]$ of desired pitch angle values. The first value is desired after 1 s and successively each value lasts for 5 s, except for the last one which lasts until the end of the experiment. To ensure correct reference tracking, for each step value and during its active period, an appropriate constant reference input $\bar{u}_k$ is added to the feedback control input, resulting in the overall control action $u_k = \mathbf{K}(\boldsymbol{\rho}_k)\mathbf{x}_k + \bar{u}_k$, where $\bar{u}_k$ is determined according to the empirical lookup table in Fig. 7, showing the necessary input voltage to supply for each pitch angle value at equilibrium. The voltage sign lacks physical meaning but indicates the actuated rotor: positive for the rotor increasing the pitch angle, negative for the rotor decreasing it.

At this point, it is possible to run the Aero experiment, leading to the vertex controllers:

$$\mathbf{K}_1^{(0)} = \begin{bmatrix} -86.1 & -39.9 \end{bmatrix}, \mathbf{K}_2^{(0)} = \begin{bmatrix} -79.6 & -55.0 \end{bmatrix}, \tag{15}$$

and the tracking results illustrated in Fig. 8, where the measured 5% settling times for each reference value are 1.2, 2.2, 2.1, 0.65, 2.0, 0.8 and 2.5 s, respectively. The Lyapunov function corresponding to this experiment is reported in Fig. 9, where V has been computed by using the tracking error instead of the raw state of the Aero. The figure shows that in this case the mismatch between model and reality is not as impactful as it was in the case of regulation to zero.

4.3.4. Some remarks on the main practical implementation aspects

The main practical difficulties encountered during data collection and experimentation are summarized as follows:

- **Choice of the sampling time T and the number of data samples N**: These two parameters are closely related, as their product determines the total data collection duration. The sampling time T should be a multiple of the natural sampling period of the plant sensors and must strike a balance between capturing relevant system dynamics and avoiding data redundancy or computational inefficiency. For example, although the Quanser Aero provides sensor readings at a default period of 0.004 s, using such a small sampling time would generate a large number of samples with minimal additional information. This is because the system dynamics do not evolve significantly at that rate, resulting in many nearly identical successive measurements. Conversely, selecting a sampling interval that is too large (e.g., 0.2 s) may result in the loss of important dynamic information. Therefore, an intermediate value, such as $T = 0.04$ seconds, was chosen as a compromise between these extremes. The number of data samples, N, should also be selected with care. Since there is no guarantee that the collected data will be sufficiently informative for identifying system dynamics, it is crucial to use a large enough sample size. Notably, increasing N does not directly impact the computational cost of the algorithm, as the data matrix $\boldsymbol{\Psi}$ used in the LMI problem has dimensions independent of N. The only additional burden is in constructing $\boldsymbol{\Psi}$, which involves straightforward matrix multiplications. This step is performed only once and does not affect the subsequent semidefinite programming problem. However, the internal structure of $\boldsymbol{\Psi}$ does

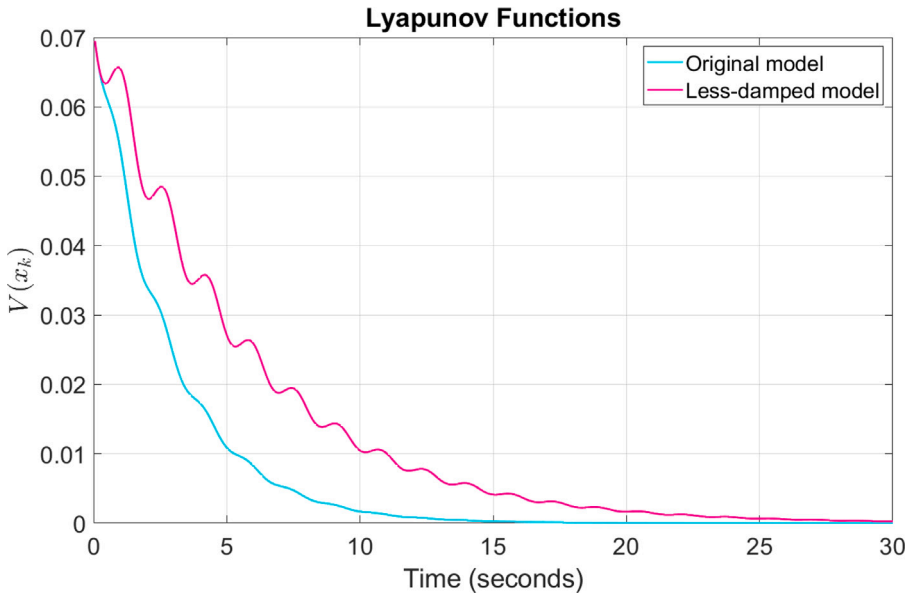

Fig. 6. Lyapunov functions corresponding to the identified LTI model and to a less-damped model assumed to be the real plant, respectively.

Pitch Angle (rad)	-0,4	-0,3	-0,2	-0,1	0	0,1	0,2	0,3	0,4
Input Voltage (Volt)	-21,7	-19,4	-16	-11,6	0	11,4	15,7	19	22,1

Fig. 7. Lookup table of the necessary input voltage to supply for each pitch angle value at equilibrium.

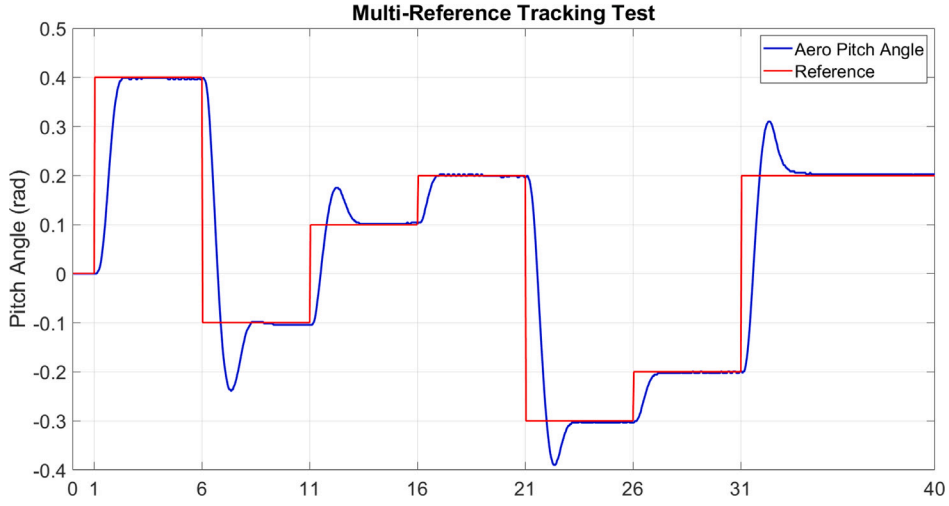

Fig. 8. Multi-step reference tracking experiment using controller in (15).

change with N, and the magnitude of its elements increases as N increases. This may lead to numerical issues or ill-conditioning in the solver. On the other hand, increasing N can improve the feasibility of the LMI, as the diagonal entries of $\boldsymbol{\Psi}$ become more negative with larger N, potentially relaxing the constraints. These considerations underscore the importance of choosing both parameters carefully to balance numerical stability, feasibility, and the informativeness of the collected data.

- **Disturbance bound** ε: This parameter should reflect the level of uncertainty in the system relative to the plant's dynamics. If ε is set too small, the LMI problem may become infeasible because the algorithm attempts to explain noisy, possibly nonlinear-affected data under an unrealistically small uncertainty assumption, making it impossible to fit any consistent linear model. Conversely, setting ε too large may also result in infeasibility. In this case, the uncertainty set becomes so broad that the resulting data-driven controller must robustly stabilize a large set of possible LTI models, which can be overly demanding or even impossible. As such, selecting an appropriate value of ε is critical to achieving feasibility. Unfortunately, no general tuning rules exist, and the

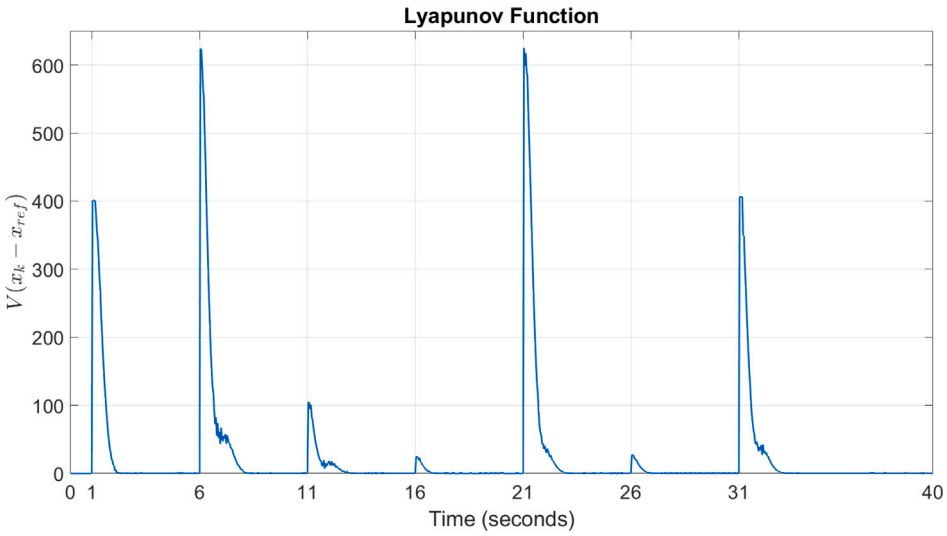

Fig. 9. Lyapunov function corresponding to the multi-step reference tracking experiment with controller in (15), where the function is computed with respect to the error variable.

user must adjust this parameter based on empirical observation and problem-specific considerations.

- **Input signal selection for the data collection**: This is the most challenging aspect, as it is essential to choose an input that excites the system at various frequencies, ideally around the resonance frequency, to ensure a rich and informative response. Possible choices include the randomly varying piecewise-constant input used here or a multi-sine waveform.

While the first three parameters, T, N and ε, typically require few trials to tune, selecting the input can be more complex, especially when determining the appropriate magnitude and phase. For instance, small magnitudes may result in weak system excitation, while large magnitudes can produce a badly-scaled data matrix, leading to numerical issues for the semidefinite programming solver. However, once the data are collected with a suitable input, the algorithm can be considered plug-and-play.

5. Conclusions

This paper has provided an in-depth analysis of the strengths and weaknesses of the data-driven LPV algorithm proposed in Miller and Sznaier (2023), highlighting its practical effectiveness with an experimental platform such as the Quanser Aero device. The experiments on the Aero have demonstrated the algorithm's ability to deliver stable control under relatively scarce information on the system dynamics, underscoring its applicability in real-world scenarios in which system modeling can be too complicated. However, the algorithm may exhibit limitations when dealing with highly nonlinear dynamics or systems with significant uncertainty.

These findings point to the need for developing a more robust version of the data-driven LPV algorithm, particularly for systems characterized by high nonlinearity or significant uncertainty. Furthermore, inspired by the approach in Verhoek, Eising, et al. (2024), exploring the use of more advanced Lyapunov functions could provide deeper insights into the algorithm's performance and potential improvements. Finally, extending the experimental validation to more complex platforms, such as the Quanser 3DOF Hover, would be a valuable direction for future work, offering a more comprehensive assessment of the methodology's scalability and robustness.

CRediT authorship contribution statement

Michelangelo Faleschini: Writing – original draft, Validation, Writing – review & editing, Formal analysis, Visualization, Investigation, Software. **Damiano Rotondo:** Supervision, Writing – review & editing, Validation, Conceptualization, Resources. **Maria Letizia Corradini:** Supervision, Project administration.

Declaration of competing interest

The authors declare that they have no known competing financial interests or personal relationships that could have appeared to influence the work reported in this paper.

References

Apkarian, P., Gahinet, P., & Becker, G. (1995). Self-scheduled H_∞ control of linear parameter-varying systems: a design example. *Automatica*, *31*(9), 1251–1261.

ApS, M. (2019). The MOSEK optimization toolbox for MATLAB manual. Version 9.0..

Bachnas, A., Toth, R., Mesbah, A., & Ludlage, J. (2014). A review on data-driven linear parameter-varying modeling approaches: A high-purity distillation column case study. *Journal of Process Control*, *24*(4), 272–285.

Becker, G., Packard, A., Philbrick, D., & Balas, G. (1993). Control of parametrically-dependent linear systems: A single quadratic Lyapunov approach. *American Control Conference*, *30*, 2795–2799.

Briat, C. (2015). Linear parameter-varying and time-delay systems. Analysis, observation, filtering & control.

Devaprakash, M., Fry, J. M., & Farhood, M. (2019). LPV control design for autonomous underwater vehicles using robustness analysis tools. *IFAC-PapersOnLine*, *52*(21), 236–241.

Inc, Q. (2016a). Quanser aero - user manual.

Inc, Q. (2016b). Quanser aero data sheet.

Khatri, C. G., & Rao, C. R. (1968). Solutions to some functional equations and their applications to characterization of probability distributions. *Sankhyā: The Indian Journal of Statistics, Series A (1961-2002)*, *30*(2), 167–180.

Liu, S., & Trenkler, O. (2008). Hadamard, Khatri-Rao, Kronecker and other matrix products. *International Journal of Information & Systems Sciences*, *4*.

Lofberg, J. (2004). YALMIP : a toolbox for modeling and optimization in MATLAB. In *IEEE international conference on robotics and automation* (pp. 284–289).

Miller, J., & Sznaier, M. (2023). Data-driven gain scheduling control of linear parameter-varying systems using quadratic matrix inequalities. *IEEE Control Systems Letters*, *7*, 835–840.

Scherer, C. W. (1996). Mixed H_2/H_∞ control for time-varying and linear parametrically-varying systems. *International Journal of Robust and Nonlinear Control*, *6*, 929–952.

Verhoek, C., Abbas, H. S., & Tóth, R. (2023). Direct data-driven LPV control of nonlinear systems: An experimental result. *IFAC-PapersOnLine*, *56*(2), 2263–2268, 22nd IFAC World Congress.

Verhoek, C., Eising, J., Dörfler, F., & Tóth, R. (2024). Decoupling parameter variation from noise: Biquadratic Lyapunov forms in data-driven LPV control. In *2024 IEEE 63rd conference on decision and control* (pp. 6761–6766).

Verhoek, C., Tóth, R., & Abbas, H. S. (2024). Direct data-driven state-feedback control of linear parameter-varying systems. arXiv:2211.17182.

van Waarde, H. J., Camlibel, M. K., Eising, J., & Trentelman, H. L. (2023). Quadratic matrix inequalities with applications to data-based control. *SIAM Journal on Control and Optimization*, *61*(4), 2251–2281.